Monitoring Lodging Extents of Maize Crop Using Multitemporal GF-1 Images

Xuzhou Qu ©, Dong Shi, Xiaohe Gu ©, Qian Sun ©, Xueqian Hu, Xin Yang, and Yuchun Pan

Abstract—Maize crop lodging is a recurrent phenomenon which results in significant reduction of grain yield and quality in addition to the impediment of mechanical harvesting. The large-scale monitoring of maize crop lodging is important for production policy adjustment and agricultural insurance compensation. In this article, we derived a variety of features from multitemporal GaoFen-1 (GF-1) images before and after maize crop lodging. We screened the most sensitive features of the spectrum, texture, and vegetation index to monitor maize crop lodging. The recursive feature elimination method based on cross-validation and mutual information were compared to obtain the optimal feature combination for monitoring the lodging extents of maize crop. The random forest classifier was used to classify the lodging extents. The results showed that the most sensitive features of the spectrum, texture, and vegetation indices of lodging extents included the difference of reflectance in blue, green, and red bands, the difference of normalized difference vegetation index, the difference of ratio vegetation index, the difference of enhanced vegetation index difference, the difference of mean value of blue band, the difference of mean value of green band, and the difference of mean value of red band. The total accuracy of lodging extents classification was 87.50%, and the Kappa coefficient was 0.83 for testing samples. Based on multiple features derived from GF-1 images before and after lodging, the lodging extents of maize crop can be monitored on a large scale.

Index Terms—Lodging, maize crop, multitemporal, random forest (RF), recursive feature elimination (RFE) method based on cross-validation (RFECV).

I. INTRODUCTION

AS ONE of the three major food crops in China, maize crop plays a critical role in grain production [1]. Lodging is a phenomenon in maize crop production, and is mainly caused by strong winds, hail, and heavy rainfall [2]. Lodging seriously

Xuzhou Qu is with the School of Geoscience, Yangtze University, Wuhan 430100, China, and also with the Research Center of Information Technology, Beijing Academy of Agriculture and Forestry Sciences, Beijing 100097, China (e-mail: 202071359@yangtzeu.edu.cn).

Dong Shi is with the School of Geoscience, Yangtze University, Wuhan 430100, China (e-mail: sdd129@126.com).

Xiaohe Gu, Qian Sun, Xueqian Hu, Xin Yang, and Yuchun Pan are with the Research Center of Information Technology, Beijing Academy of Agriculture and Forestry Sciences, Beijing 100097, China (e-mail: guxh@nercita.org.cn; sunq817@163.com; huxq@sdust.edu.cn; 15803304826@163.com; panyc@nercita.org.cn).

affects the photosynthesis, nutrient, and water transport of maize crop, and makes the plant more vulnerable to diseases and insect pests, resulting in the reduction in maize crop yield [3], [4]. Maize lodging causes nearly 15%–30% yield on an average, and it can reach up to 50% or even total loss in case of severe lodging (SL) case [2]. Therefore, the timely and accurate monitoring of maize crop lodging is beneficial to assess the growth status of maize crop for agricultural departments, which provide a powerful data for agricultural insurance claims of farmers [5] and adjust agricultural production policy [6].

In traditional crop lodging monitoring, lodging information is mostly obtained from field observation, subjected to expert knowledge and subjectivity [7]. Remote sensing technology has the advantages of rapid and all weather application, and provides objective information [8]. Remote sensing technology can be applied to achieve rapid, objective, and large-scale monitoring of crop lodging [9]. Crop lodging cause changes in the canopy structure, radiation use efficiency of the crop canopy, and its spectral characteristics. Therefore, crop lodging information can be extracted by comparing the differences in spectral reflectance, texture, and plant height between lodged and nonlodged plants [10]. The canopy reflectance is mainly obtained by spectrometry, hyperspectral remote sensing, multispectral remote sensing, and other means to analyze the spectral reflectance differences between lodging and nonlodging (NL) crops [11]. The texture features extracted by the method of local binary patterns and gray-level co-occurrence matrix (GLCM) [12] are used to describe the relationships of ground objects with surrounding ground objects [13]. The textural features with significant differences between lodging and NL crops can be found, and crop lodging distributions can be identified. The canopy height of crops can be obtained using LiDAR, ultrasonic waves, depth cameras, and visible light cameras. The height difference can be used to identify between lodging and NL crops [14]–[16].

At present, scholars have conducted many studies on monitoring crop lodging. In the field experiment, digital cameras and spectrometers were widely used in lodging research [17]. For example, digital cameras were used to monitor rice lodging [8]. Based on the analysis of canopy spectral reflectance, principal component analysis and artificial neural network (ANN) [18] were used to monitor rice lodging. With the development of unnamed aerial vehicles (UAVs) and satellite remote sensing, the methods of monitoring crop lodging become more diversified [19]–[21]. The spectrum, texture, color, and topographic

information obtained from UAV images are important features of monitoring crop lodging [6], [22], [23]. Moreover, from UVA images, the method of combining structure-from-motion with geostatistics [24] and particle swarm optimization combined with supporting vector machine (SVM) [25] made crop lodging monitoring more precise. Whether field experiment or UAV, it will spend a lot of time and manpower for large-scale crop lodging monitoring [8], [12], [26]–[28]. Synthetic aperture radar (SAR) can overcome the influences of clouds and shadows. A few studies have explored crop lodging from different perspectives [29], [30]. Zhao *et al.* [31] used a series of polarized SAR (PolSAR) to explore the ability of monitoring lodging in wheat and rape. It was found that the lodging monitoring ability of PolSAR was related to the canopy structure of crops. The radar polarization index derived from Radarsat-2 image data could be used to monitor wheat lodging [32]. The changes of canopy height before and after lodging were also used to monitor the lodging of crops [33], [34]. Chauhan *et al.* [35] estimated the lodging angle by Sentinel-1 and Radarsat-2, and evaluated the lodging degree of crops. At present, optical satellites images have been applied in crop lodging monitoring. Chen *et al.* [36] proposed a spectral sum index to identify the lodging range of large-scale maize crop by analyzing the spectral changes of NL and lodging maize crop. These studies [36], [37] mainly focused on the monitoring of lodging range of crops. Therefore, the evaluation of large-scale lodging extents is of great significance. Machine learning methods, such as SVM [25], ANN [18], and random forest (RF) [37], [38], were widely used in crop lodging monitoring. Among them, RF was used most frequently and had the highest accuracy.

Selecting effective feature combination is helpful to improve the accuracy and efficiency of crop lodging monitoring. Feature selection algorithms can be divided into three categories: filter, wrapper, and embedding. The filter algorithms appeared first, of which the process is independent of the classifier [39]. Its main algorithms include the Pearson correlation coefficient and the mutual information (MI) criterion [39]. The calculation processes of these algorithms are simple and quick. Wrapper algorithms select the feature subset that is most beneficial to the performance of a given learner, but its computation burden is huge [40]. Embedding algorithms are integrated with the classifier, and the optimal feature is selected in the learning process of the learner [41]. For example, the decision tree algorithm performs feature screening when the optimal variables of the tree nodes are automatically selected. The recursive feature elimination (RFE) algorithm combines the advantages of wrapper and embedding algorithms, and is more closely combined with the learner, which is more conducive to feature selection [42].

Based on GaoFen-1 (GF-1) image and statistical analysis methods, and combined with field samples, the article aimed to find sensitive features in the spectrum, texture, and vegetation indices to monitor maize crop lodging. Recursive feature elimination based on cross-validation (RFECV) and MI were used to select the best feature combination for sensitive features. Then, we achieved the classification of lodging extents using an RF classifier. The purpose of this article was to provide a technical reference for monitoring maize crop lodging.

II. DATA SOURCE

A. Overview of the Study Area

Lishu County, Siping City, Jilin Province is located in the Songliao Plain with geographic coordinates of 123°45'–124°53'E and 43°02'–43°46'N. It has a north, temperate, semi-humid, continental monsoon climate with simultaneous rain and heat, and four distinctive seasons. In 2016–2020, the planting area of maize crop in Lishu County was approximately 200 000 hectares, accounting for 90% of the total grain planting area. The annual output of maize crop was approximately 2 million tons, accounting for more than 90% of the total grain output in the county. Maize crop is important for grain production in Lishu County.[1] In recent years, severe meteorological disasters such as spring droughts, summer waterlogging, strong winds, and heavy rainfall have occurred in the county, which have seriously affected the sustained and stable yield of maize crop. Lodging, caused by strong winds and heavy rainfall, is an important factor for maize yield reduction. The location of the study area and the distribution of the field samples in Lishu County are shown in Fig. 1.

B. Data Acquisition

On August 27 and September 3, 2020, Jilin Province was affected by Typhoons Bavi and Maysak, which led to large-scale maize crop lodging in Lishu County. Typhoon information came from the typhoon network of China Meteorological Observatory.[2] The spatial resolution of digital elevation data is 30 m.[3] The path and magnitude of the typhoon are shown in Fig. 2. The meteorological data was obtained from August 25th to September 6th from the Central Meteorological Network in Table I.[4] In this article, we selected two GF-1 WFV images, before and after lodging as data sources. The parameters of the satellite data are listed in Table II.[5] The imaging dates were August 16, 2020 (before lodging) and September 6, 2020 (after lodging). According to Table III, the two remote sensing images were at the filling stage, which is the key period of formation of maize yield. Atmospheric correction, orthocorrection, geometric correction, clipping, mosaic, and stitching operations were performed on the GF-1 images in ENVI 5.3.

On September 6, 2020, maize crop plots with 30 m × 30 m were randomly selected for field investigation. A portable decimeter GPS (Trimble GeoXH2008) was used for positioning. The lodging rate was estimated by agronomic experts in the field. Similarly, nonmaize samples were collected, including building, water, forest, rice, and bare soil. There were 100 maize crop and 69 nonmaize samples.

---

[1][Online]. Available: http://www.stats.gov.cn
[2][Online]. Available: http://typhoon.nmc.cn/web.html
[3][Online]. Available: https://search.earthdata.nasa.gov
[4][Online]. Available: http://weather.cma.cn/
[5][Online]. Available: http://www.cresda.com/CN/Satellite/3076.shtml
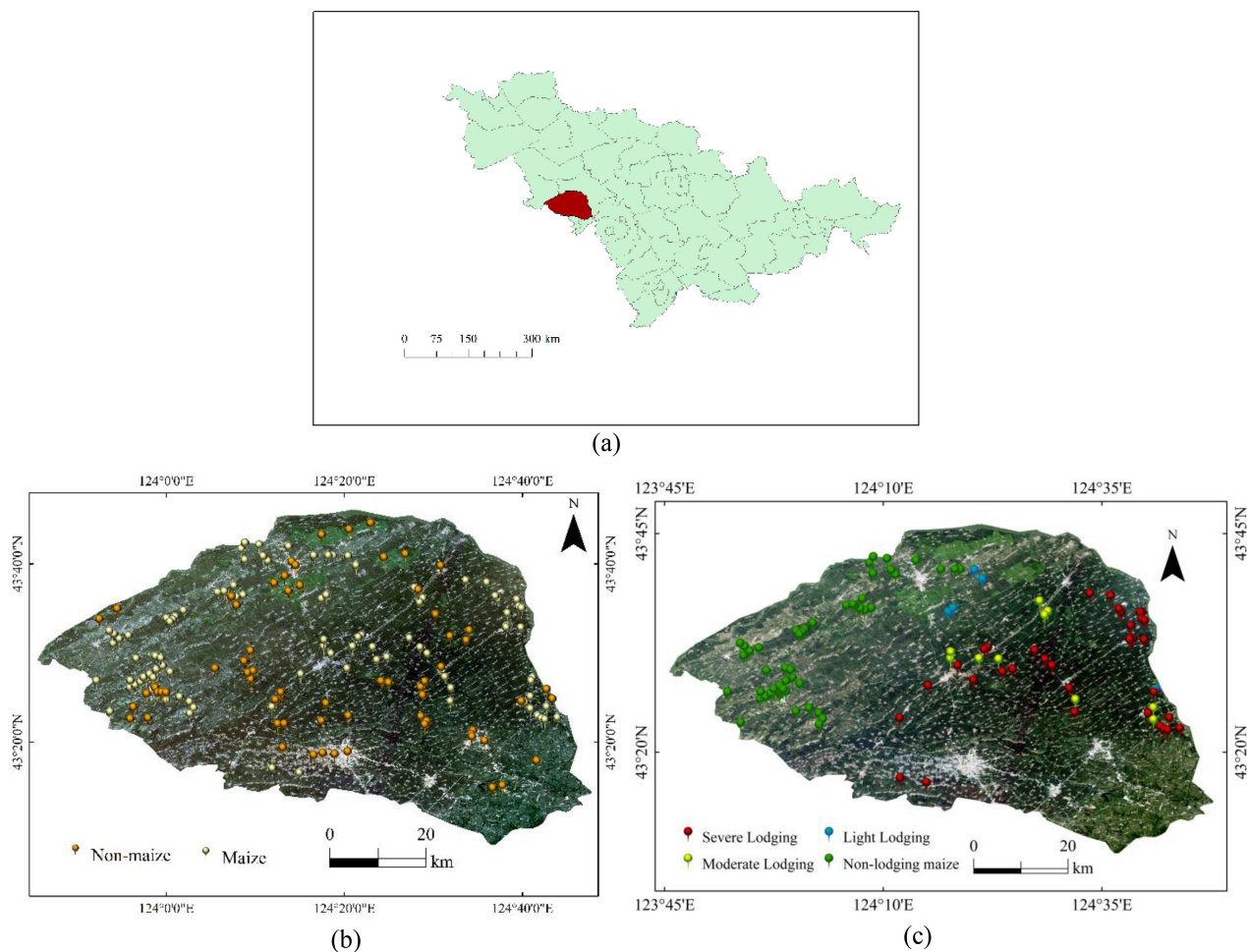
(a)

(b)

(c)

Fig. 1.   Location of study area and distribution of field samples. (a) Location of study area. (b) Distribution of maize crop and nonmaize samples. (c) Distribution of maize crop extents samples.
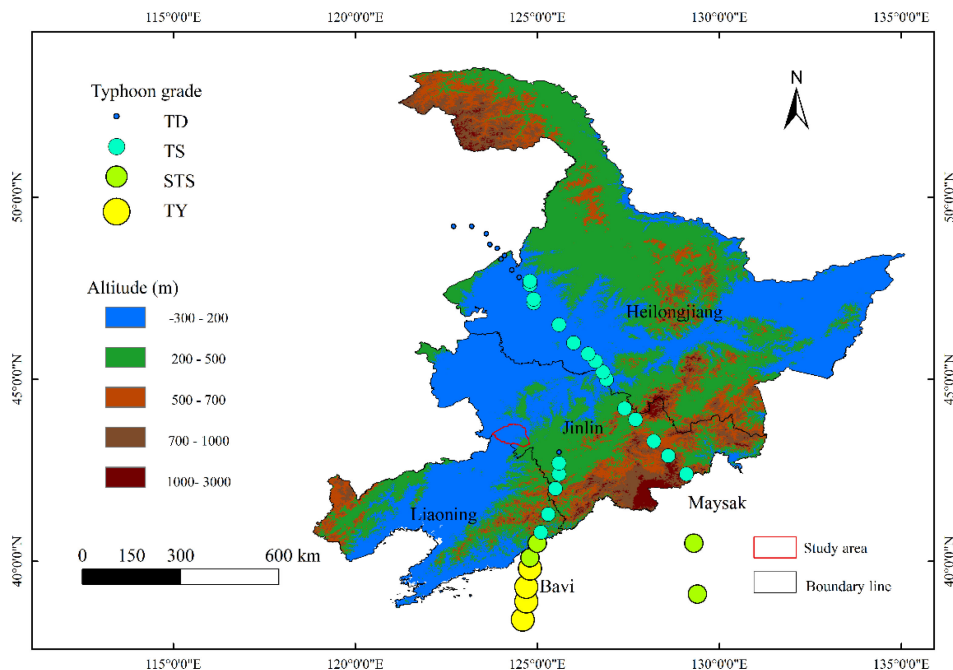

Fig. 2.   Typhoon track. TD: tropical depression, TS: tropical storm, STS: severe tropical storm, and TY: typhoon.

TABLE I
METEOROLOGICAL CONDITIONS OF LISHU COUNTY

| Time	Weather condition	Wind direction/ wind force	Time	Weather condition	Wind direction/ wind force
2020.08.25	Cloudy	NW/1-2	2020.09.01	Cloudy	SW/3-4
2020.08.26	Light rain	NW/3-4	2020.09.02	Light rain	N/4-5
2020.08.27	Heavy rain	NW/1-2	2020.09.03	Rainstorm	N/6-8
2020.08.28	Light rain	SW/1-2	2020.09.04	Cloudy	W/4-5
2020.08.29	Light rain	SW/1-2	2020.09.05	Light rain	SW/3-4
2020.08.30	Cloudy	SW/1-2	2020.09.06	Cloudy	SW/1-2
2020.08.31	Light rain	SW/1-2			
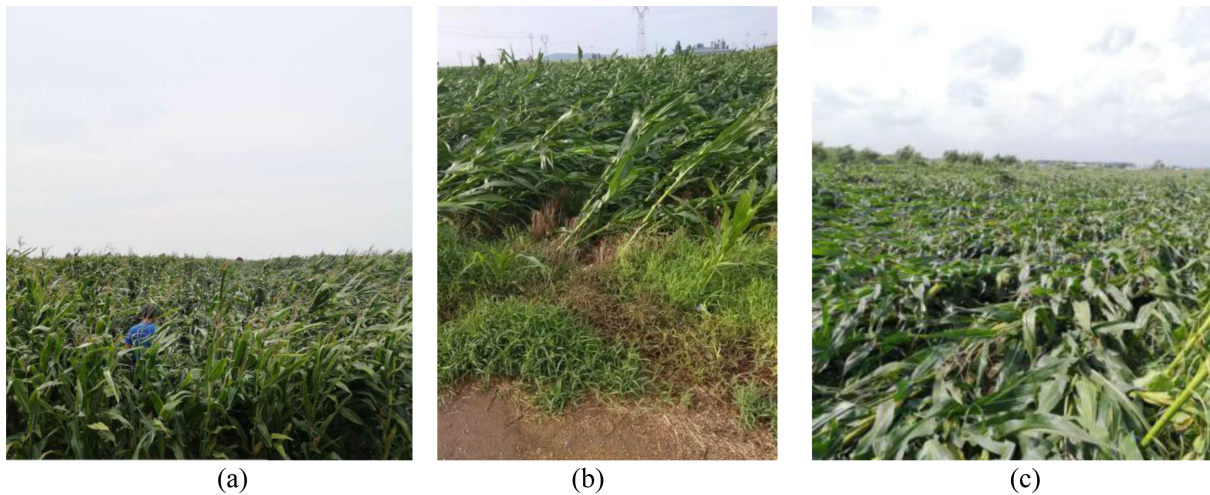
Fig. 3. Photos of maize crop lodging in Lishu County. (a) Light lodging. (b) Moderate lodging. (c) Severe lodging.

TABLE II
PHENOLOGICAL INFORMATION OF MAIZE CROP IN LISHU COUNTY

Stage	Date
Sowing	Late April – Early May
Seedling	Middle May – Early June
Jointing	Middle June – Early July
Silking	Middle July – Early August
Filling	Middle August – Early September
Harvesting	Middle September – Late September

The lodging ratio per unit area was divided into 0%–10%, 11%-60%, 61%–90%, and 91%–100% [38], which correspond to NL, light lodging (LL), moderate lodging (ML), and SL, respectively. Finally, we obtained 35 SL, 10 ML, 5 LL, and 50 NL samples. Photos of maize crop lodging are shown in Fig. 3.

III. RESEARCH METHODS

A. Technical Process

The technical process of this article is shown in Fig. 4. The main steps are as follows:

1) The supervised classification method was used to extract the spatial distribution of maize crops from the GF-1
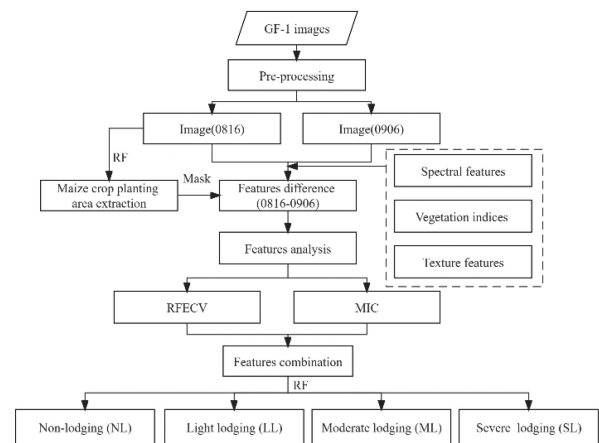

Fig. 4. Technical flowchart.

images on August 16, which were declouded based on the image of September 6.

2) Based on GF-1 images after maize crop masking, the spectral, vegetation indices, and texture features were calculated, and the features that were different before and after lodging were constructed.

3) A method based on statistical analysis was used to analyze the features with differences, and the features sensitive to lodging extents were screened.

TABLE III
REMOTE SENSING DATA PARAMETERS OF THE GF-1 SATELLITE

Platform	Sensor	Central wavelength/nm	Wavelength range/nm	Acquisition date	Cloud coverage/%	Spatial resolution	Revisit period	Swath width
GF-1	WFV3	485	450–520	August 16	0	16 m	4 days	800 km
		555	520–590					
		660	630–690					
		830	770–890					
	WVF4	485	450–520	September 6	6			
		555	520–590					
		660	630–690					
		830	770–890					

TABLE IV
CALCULATION FORMULA OF VEGETATION INDICES

Vegetation index	Calculation formula	Reference
Normalized difference vegetation index (NDVI)	$\dfrac{(R_{nir} - R_{red})}{(R_{nir} + R_{red})}$	[50]
Ratio vegetation index (RVI)	$\dfrac{R_{nir}}{R_{red}}$	[51]
Atmospherically resistant vegetation index (ARVI)	$\dfrac{(R_{nir} - (2 \times R_{red} - R_{blue}))}{(R_{nir} + (2 \times R_{red} - R_{blue}))}$	[52]
Enhanced vegetation index (EVI)	$2.5 \times \dfrac{(R_{nir} - R_{red})}{(R_{nir} + 6 \times R_{red} - 7.5 \times R_{blue} + 1)}$	[53]
Structure insensitive pigment index (SIPI)	$\dfrac{(R_{nir} - R_{blue})}{(R_{nir} - R_{red})}$	[54]

4) RFECV and MI were used to optimize the features, and the optimal feature combination of lodging extents was obtained.
5) The RF classifier was used to classify the optimal feature combination, and the extents of the lodging were obtained.

B. Feature Construction

For the spectral features, after preprocessing the remote sensing image, we obtained the reflectance of four bands, including the reflectance of the blue band (R_{blue}), green band (R_{green}), red band (R_{red}), and near infrared band (R_{nir}).

For the features of the vegetation indices, we selected five vegetation indices [30], [43]–[47]. Their calculation formulas are listed in Table IV.

For texture features, we calculated the GLCM of the spectral image with a 3×3 filtering window [48], [49] and a moving direction of $45°$ after comparing with other kernels and directions. Eight texture features were calculated, including mean, variance, homogeneity, dissimilarity, contrast, entropy, correlation, and second moment. Their calculation formulas are listed in Table V.

For the difference features, we subtracted the spectral, vegetation indices, and texture features after lodging from those before lodging. The calculation formula used is shown as

$$\Delta T = T_{Aug.16} - T_{Sep.6} \qquad (1)$$

where ΔT is the difference features, $T_{Aug.16}$ is the features of the remote sensing images on August 16, and $T_{Sep.6}$ is the features of the remote sensing images on September 6.

The values of each difference feature were extracted by field samples of maize crop. We used these values to generate a box plot, and then observed the differences between different states of maize crop. One-way analysis of variance with post-hoc comparisons (Games–Howell Post-hoc test [55], which assumes unequal variance between groups) was used to find the significant pairwise differences among the classes. Significance was calculated in SPSS software (version 20.0; SPSS Inc.,

TABLE V
TEXTURE FEATURE CALCULATION FORMULAS

Texture feature	Formula	Abbreviation	Texture abbreviation of each band	Reference
Mean	$\sum_{i}\sum_{j} p(i,j) \times i$	MEA	B_MEA, G_MEA, R_MEA, NIR_MEA	
Variance	$\sum_{i}\sum_{j} p(i,j) \times (i - \bar{i})^2$	VAR	B_VAR, G_VAR, R_VAR, NIR_VAR	
Homogeneity	$\sum_{i}\sum_{j} p(i,j) \times \frac{1}{1 + (i\text{-}j)^2}$	HOM	B_HOM, G_HOM, R_HOM, NIR_HOM	
Contrast	$\sum_{i}\sum_{j} p(i,j) \times (i\text{-}j)^2$	CON	B_CON, G_CON, R_CON, NIR_CON	[12]
Entropy	$\sum_{i}\sum_{j} p(i,j) \times \log_2 p(i,j)$	ENT	B_ENT, G_ENT, R_ENT, NIR_ENT	
Second Moment	$\sum_{i}\sum_{j} p(i,j)^2$	SEM	B_SEM, G_SEM, R_SEM, NIR_SEM	
Correlation	$\sum_{i}\sum_{j} \frac{(i - \bar{i}) \times (j - \bar{j}) \times p(i,j)^2}{\sigma_i \sigma_j}$	COR	B_COR, G_COR, R_COR, NIR_COR	
Dissimilarity	$\sum_{i}\sum_{j} p(i,j) \times |i - j|$	DIS	B_DIS, G_DIS, R_DIS, NIR_DIS	

where B: blue band, G: green band, R: red band, NIR: near infrared band, i, j: gray level of the pixel, i: mean value of pixel i, ρ: variance of the pixels, $p(i, j)$: the probability of the occurrence of i, j. C. Feature analysis method.

Chicago, IL, USA). The Games–Howell test corrects the degree of freedom of the *t*-test based on Welch's [55].

D. Feature Combination Optimization of RFECV and MI

The RFECV is an effective method for feature combination screening [56]. The first stage is the RFE, which is used for finding the optimal feature subset. The RF was used as the estimator of RFE. When the dataset was input into the model, the importance of each feature could be calculated based on the mean decrease of impurity (MDI). More information on MDI and feature importance evaluation with RF can be found elsewhere [57]. The model is repeatedly built to exclude the least important features [58]. This process is repeated on the remaining features to rank the importance of all features. The next stage is the cross-validation (CV) [59]. Different numbers of features were selected based on the importance of features determined in RFE stage. The CV method was used to verify the selected feature set. The number of features with the highest average score was determined [60], and the optimal feature combination was obtained. The five-fold CV was used in the article.

In feature selection, MI [61] is to find features that are highly related to the class and have low redundancy between features. Its principle is simple and its calculation speed is fast. However, if there is a high correlation between features, the algorithm can easily lead to the redundancy of feature variables. The MI can be calculated as formula (2). First, MI was used to evaluate the importance of input features, and then the method of CV was used to verify the selected feature set. The number of features with the highest average score was determined, and the feature selection was completed. Both RFECV and MI were

implemented in Python (version 3.8)

$$I\ (X, Y) = \sum_{y \in Y}\sum_{x \in X} p\ (x, y) \log \left(\frac{p\ (x, y)}{p\ (x)\, p\ (y)} \right). \quad (2)$$

For two random variables X and Y, their joint probability density function is $p\ (X, Y)$, the marginal probability density function is $p\ (Y)$ and $p\ (Y)$, and $I\ (X, Y)$ is the MI.

E. RF Classifier

RF is a classifier that uses multiple trees to train and predict the samples [62]. Each decision tree is a classifier. For an input sample, n trees generate n classification results [63]. The RF integrates all the classified voting results and designates the category with the most votes as the final output. Compared to other nonparametric classifiers, RF has a faster calculation speed and lower cost [64]. RF can deal with high-dimensional data, has strong anti-interference ability, and strong anti-over-fitting ability [65]. In this article, the RF classifier of ENVI 5.3 [66] was used to extract and classify the maize crop. The parameter settings were as follows: number of trees is 100, number of features is square root, and impurity function is Gini coefficient.

F. Lodging Classification Method

The algorithms of RFECV and MI were used to optimize all features, respectively. After comparison, the most sensitive feature combination for lodging extents of maize crop was obtained. 3/5 of all field samples were randomly used to train the models and the remaining samples were used to validation. We used the training samples to train the RF classifier. The extents of lodging were obtained. We verified classification

TABLE VI
SEPARABILITY OF TRAINING SAMPLES

Class	Rice	Forest	Water	Building	Bare soil	Maize crop
Rice		1.955	2.000	1.999	2.000	1.999
Forest	1.955		1.965	1.989	1.999	1.999
Water	2.000	1.965		1.990	1.975	2.000
Building	1.999	1.989	1.990		1.975	1.998
Bare soil	2.000	1.999	1.975	1.975		2.000
Maize crop	1.999	1.999	2.000	1.998	2.000	

TABLE VII
CONFUSION MATRIX OF MAIZE CROP EXTRACTION

	Training samples			Testing samples		
Class	Maize crop	Non maize crop	Total	Maize crop	Non maize crop	Total
Maize crop	98	0	98	89	0	89
Non maize crop	2	82	84	11	69	80
Total	100	82	182	100	69	169
	TA: 98.90%, K: 0.98			TA: 93.49%, K: 0.87		

Total accuracy: TA, Kappa Coefficient: K.

accuracy by calculating the confusion matrix with the testing samples.

IV. RESULTS

A. Extraction of Maize Crop Planting Area

The cloud distribution was extracted from GF-1 image on September 6 to obtain the cloudless region of the two-phase images. The training samples were randomly selected from Google high-resolution images, including 100 maize and 82 nonmaize samples. The separability of training samples was above 1.90 in Table VI. After comparing two classifiers, the RF was used to classify the imagery of removing cloud on August 16. The testing samples included 100 maize crop samples and 69 nonmaize samples. The total accuracy of training samples was 98.90% and Kappa coefficient was 0.98. The total accuracy of testing samples was 93.49% and Kappa coefficient was 0.87. The confusion matrix of maize crop extraction is shown in Table VII. The maize distribution is shown in Fig. 5. According to the official report of Lishu County, the maize crop planting area was 210 000 hectares in 2020.[6] The maize crop planting area by classification is 203 500 hectares, which is 6500 hectares less than the official report (3%). This is caused by the removal of the area where clouds exist in planting area. This accuracy met the requirements for our subsequent research in this article.

B. Spectral Features Analysis

Fig. 6 shows the mean and standard deviation of reflectance between lodging and NL maize crop samples obtained from the image on September 6. The mean and standard deviation of R_{blue}
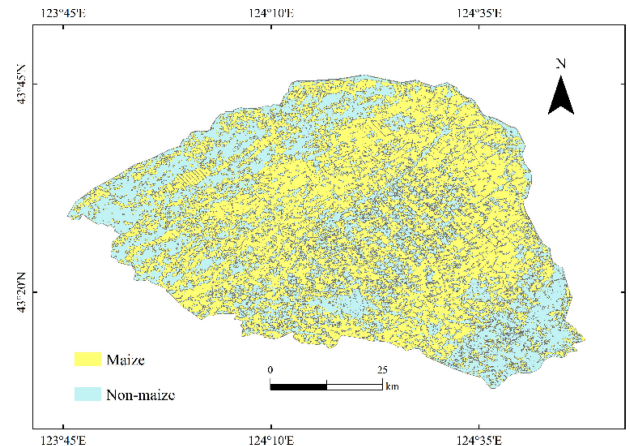
Fig. 5. Spatial distribution of maize crop.

(485 nm), R_{green} (550 nm), R_{red} (660 nm), and R_{nir} (830 nm) of lodging maize were higher than NL maize. Because the canopy height of maize crop decreased after lodging and the canopy structure of maize crop considerably changed, which led to a significant change in the proportion of stalks and leaves in the view of the maize crop canopy spectrum [15], the reflectance of maize crop stalk is higher than that of leaf. The more serious the lodging, the higher the straw exposure [67], and higher the reflectance (Fig. 6).

The quartile is the value of a set of data sorted at 25% and 75%. The description of the data in the quartile interval can more effectively represent the characteristics of the data and eliminate the interference of data outliers. We used field samples to extract the difference of spectral reflectance. The ML and SL in ΔR_{blue}, ΔR_{green}, and ΔR_{red} are obviously separated from

TABLE VIII
POST-HOC GAMES–HOWELL *P*-VALUE STATISTICS OF DIFFERENT LODGING EXTENTS FOR DIFFERENCE OF REFLECTANCE

Class pairs	ΔR_{BLUE}	ΔR_{GREEN}	ΔR_{RED}	ΔR_{NIR}
NL–LL	2.845×10^{-1}	3.060×10^{-1}	2.148×10^{-1}	9.897×10^{-1}
NL–ML	$\mathbf{2.000\times10^{-4}}$***	$\mathbf{5.000\times10^{-4}}$***	$\mathbf{4.000\times10^{-4}}$***	5.100×10^{-1}
NL–SL	$\mathbf{6.682\times10^{-13}}$***	$\mathbf{1.174\times10^{-12}}$***	$\mathbf{8.467\times10^{-13}}$***	9.991×10^{-1}
LL–ML	2.651×10^{-1}	3.121×10^{-1}	3.038×10^{-1}	1.455×10^{-1}
LL–SL	7.040×10^{-2}	7.310×10^{-2}	5.080×10^{-2}	9.999×10^{-1}
ML–SL	4.241×10^{-1}	4.684×10^{-1}	3.425×10^{-1}	3.541×10^{-1}

*, **, and *** indicate 0.05, 0.01, and 0.001 levels of significance.
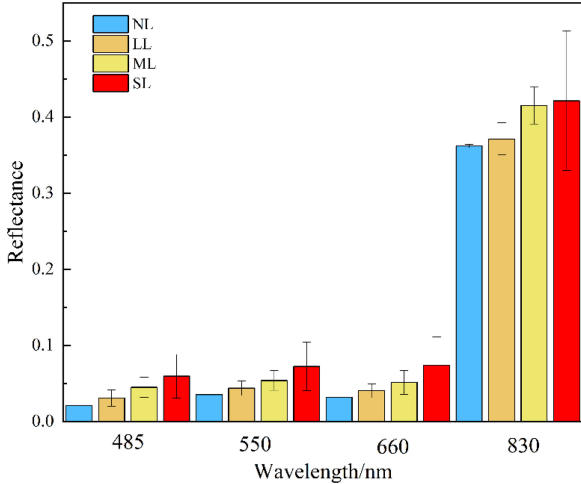
Fig. 6. Mean and standard deviation of reflectance between lodging and nonlodging maize crop.

the quartile of NL and LL, while the separability of NL, LL, ML, and SL in ΔR_{nir} is not obvious in Fig. 7(a). The Post-hoc Games–Howell (pairwise) test comparison identified significant differences between NL and ML and between NL and SL (for ΔR_{blue}, ΔR_{green}, and ΔR_{red}) in Table VIII. Among the four features, ΔR_{blue}, ΔR_{green}, and ΔR_{red} show good separability in the lodging extents, while the ΔR_{nir} before and after lodging is not obvious. This is consistent with the conclusion in [44], [67].

Through the analysis of the spectral, we found that the sensitive characteristics of the lodging extents of maize crop were ΔR_{blue}, ΔR_{green}, and ΔR_{red}.

C. Vegetation Index Analysis

The vegetation indices before and after lodging using field samples were obtained. Because the scales of ΔNDVI, ΔRVI, ΔEVI, ΔARVI, and ΔSIPI were different, the five vegetation indices were compared by calculating the change rate before and after lodging, as shown in Fig. 7(b). The relative change of lodging was calculated as

$$\text{VI}_c = \frac{\text{VI}_b - \text{VI}_a}{\text{VI}_b} \tag{3}$$

where VI_c is the change rate of vegetation index before and after lodging, and VI_b and VI_a are the vegetation indices before after lodging, respectively.

In Fig. 8, there is a significant difference in quartile between the NL of NDVI, RVI, and EVI, and the other three lodging

extents. LL and SL of NDVI and RVI are separable in quartile. The Post-hoc Games–Howell (pairwise) test comparison identified significant differences between NL and ML (for ΔNDVI, ΔRVI, and ΔEVI), between NL and SL (for ΔNDVI, ΔRVI, and ΔEVI), and between LL and SL (for ΔNDVI and ΔEVI) in Table IX. After lodging, the canopy structure of maize crop changed significantly, which led to significant changes in the leaf area index [68] and canopy reflectance of the maize crop. Therefore, ΔNDVI, ΔRVI, and ΔEVI, which are sensitive to changes in canopy structure, produced better effects in distinguishing the grade of lodging maize crop. SIPI is generally used to maximize the sensitivity of the carotenoid-to-chlorophyll ratio when the canopy structure decreases and is sensitive to pigment changes. Remote sensing images were acquired on the third day after lodging. Because the change of chlorophyll content was small, SIPI was unable to distinguish the lodging extents of maize crop.

Through the analysis of the vegetation index, we found that the sensitive characteristics that can distinguish the extents of lodging maize crop were ΔNDVI, ΔRVI, and ΔEVI.

D. Texture Feature Analysis

The differences of texture features were extracted by field samples, which were analyzed by box plot and Games–Howell significance test. Among all the differences of texture features, only the ΔB_MEA, ΔG_MEA, and ΔR_MEA have obvious separability between NL and other lodging extents in Fig. 8. ΔG_MEA and ΔR_MEA have obvious separability in all lodging extents. There is a partial overlap between SL and ML of ΔB_MEA. The Post-hoc Games–Howell (pairwise) test comparison identified significant differences between NL and ML (ΔB_MEA, ΔG_MEA, and ΔR_MEA), between NL and SL (ΔB_MEA, ΔG_MEA, and ΔR_MEA), between LL and SL (ΔB_MEA, ΔG_MEA, and ΔR_MEA), and between ML and SL (ΔR_MEA) in Table X. In summary, the texture features that distinguished the sensitivity of lodging maize were ΔB_MEA, ΔG_MEA, and ΔR_MEA.

E. Evaluating Maize Crop Lodging Grades

All the difference features extracted from the field samples were put into RFECV and MI for screening sensitive features, respectively. Fig. 9 shows the results of RFECV and MI feature screening. The highest accuracy of RFECV is 95.00% when nine features are selected for the first time. The highest accuracy of MI is 93.00% and the number of features is 33. The result of RFECV was taken as the result of feature combination screening. These
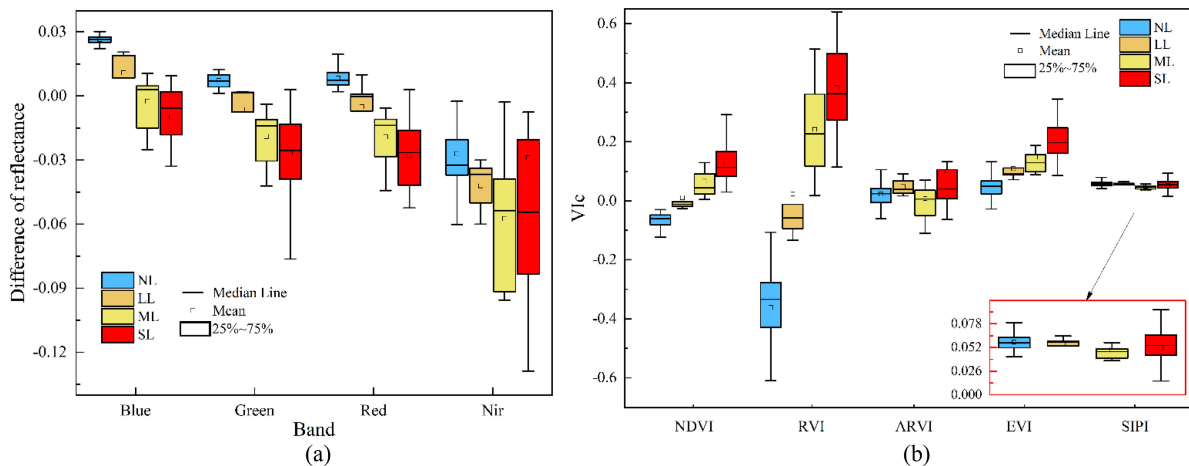
Fig. 7.   Changes in the reflectance and vegetation indices in different lodging extents. (a) Difference of reflectance. (b) VI_c of five vegetation indices.
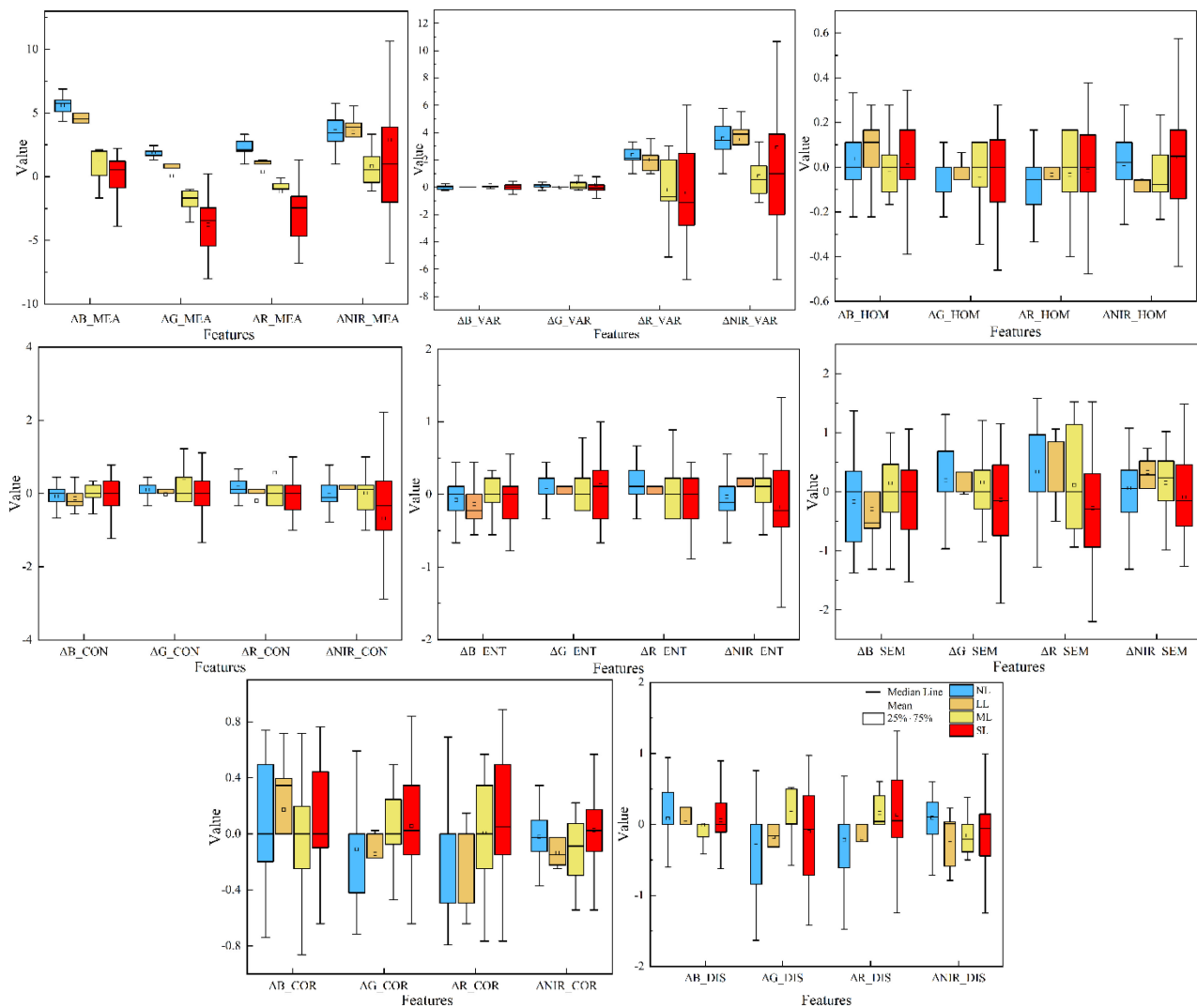

Fig. 8.   Changes in the texture characteristics of different lodging extents before and after lodging.

TABLE IX
POST-HOC GAMES-HOWELL *P*-VALUE STATISTICS OF DIFFERENT LODGING EXTENTS FOR VI$_c$

Class pairs	ΔNDVI	ΔRVI	ΔEVI	ΔARVI	ΔSIPI
NL–LL	$1.446×10^{-1}$	$1.209×10^{-1}$	$9.570×10^{-2}$	$3.057×10^{-1}$	$9.289×10^{-1}$
NL–ML	**$8.000×10^{-4}$***	**$2.800×10^{-5}$***	**$3.000×10^{-3}$**	$9.678×10^{-1}$	$3.280×10^{-1}$
NL–SL	**$6.485×10^{-13}$***	**$5.802×10^{-13}$***	**$5.624×10^{-13}$***	$3.210×10^{-1}$	$5.757×10^{-1}$
LL–ML	$3.974×10^{-1}$	$3.462×10^{-1}$	$5.475×10^{-1}$	$5.639×10^{-1}$	$6.706×10^{-1}$
LL–SL	**$3.010×10^{-2}$***	$1.040×10^{-1}$	**$2.19×10^{-2}$***	$3.339×10^{-1}$	$9.071×10^{-1}$
ML–SL	$9.630×10^{-2}$	$3.696×10^{-1}$	$1.445×10^{-1}$	$1.036×10^{-1}$	$9.653×10^{-1}$

*, **, and *** indicate 0.05, 0.01, and 0.001 levels of significance.
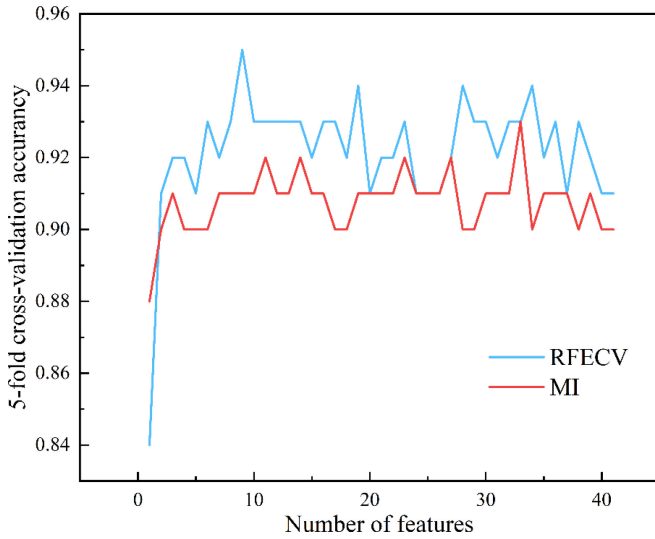
Fig. 9. Plot of feature screening based on RFECV and MI.

Fig. 10. Classification of lodging extents.

nine features are ΔR_{blue}, ΔR_{green}, ΔR_{red}, ΔNDVI, ΔRVI, ΔEVI, ΔB_MEA, ΔG_MEA, and ΔR_MEA, respectively. The result of RFECV is consistent with that of feature analysis. So the optimal combination of feature was ΔR_{blue}, ΔR_{green}, ΔR_{red}, ΔNDVI, ΔRVI, ΔEVI, ΔB_MEA, ΔG_MEA, and ΔR_MEA.

The RF classifier was used to classify the optimal feature combination, and a confusion matrix to verify the accuracy of the lodging classification. The accuracy of training samples was 95.00%, kappa coefficient was 0.93, and the accuracy of testing samples was 87.50%, kappa coefficient was 0.83. The confusion matrix of lodging extents classification is in Table XI. According to the confusion matrix, one of the SL testing samples were mistakenly classified as ML, and one of the ML maize crop testing samples was mistakenly classified as SL. The three samples of NL were mistakenly divided into LL. The maize crop status of NL, LL, ML, and SL is similar. They have more complex lodging at the junction, resulting in incorrect division. Through the classification of lodging extents, we could quickly judge the scope and extents of lodging and master the lodging situation of the whole region. This can help agricultural departments perform policy adjustments and with
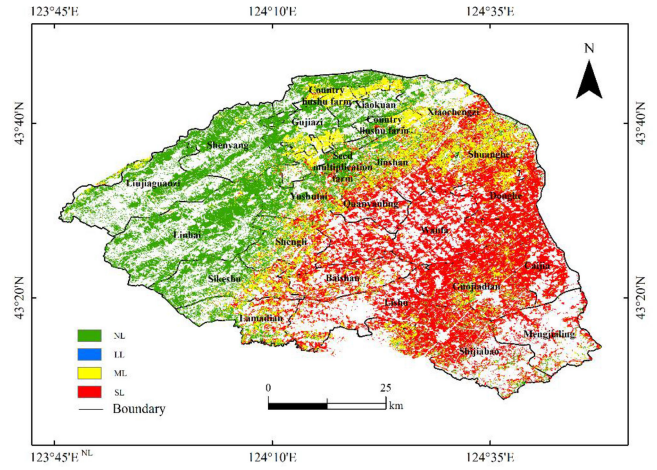
related agricultural insurance compensation. The results of the lodging extents classification are shown in Fig. 10.

The SL was mostly concentrated in the central and eastern of Lishu County, accounting for a large proportion of the total lodging. In Quanyanling Town, Wanfa Town, Donghe Town, Caijia Town, the east of Lishu Town, and the south of Yushutai Town, the area of SL was larger than the other three lodging extents. LL was mainly distributed in the north of Lishu County, covering only a small area. The statistical results of the lodging extents of maize crop in the towns are shown in Fig. 11. A large proportion of SL and ML was in the central and eastern parts of Lishu County. Most of LL was in the north of Lishu County.

When the typhoon passed, there was heavy rain and strong winds in Lishu County in Table I. The lodging of maize crop in Lishu County was caused by Typhoons Bavi and Maysak. The paths of the typhoons are illustrated in Fig. 2. When Bavi approached from the south of Jilin, the Changbai Mountains served as a barrier between Lishu and the typhoon, weakening the impact of strong winds. After entering Jilin, the winds gradually weakened, so Bavi only had a slight impact on Lishu. Bavi had a greater effect on the maize crop in the southeast than in the northwest of Lishu. Maysak approached from the southeast of Jilin. The winds were strong and long-lasting. The

TABLE X
POST-HOC GAMES–HOWELL *p*-VALUE STATISTICS OF DIFFERENT LODGING EXTENTS FOR DIFFERENCE OF TEXTURE

Class pairs	ΔB_MEA	ΔG_MEA	ΔR_MEA	ΔNIR_MEA	ΔB_VAR	ΔG_VAR	ΔR_VAR	ΔNIR_VAR	ΔB_HOM	ΔG_HOM	ΔR_HOM	ΔNIR_HOM
NL-LL	3.240×10^{-1}	2.78×10^{-1}	1.72×10^{-1}	9.997×10^{-1}	9.980×10^{-1}	8.670×10^{-1}	9.647×10^{-1}	8.771×10^{-1}	9.865×10^{-1}	9.983×10^{-1}	9.508×10^{-1}	5.746×10^{-1}
NL-ML	$\mathbf{9.000\times10^{-6}}$***	$\mathbf{7.000\times10^{-6}}$***	$\mathbf{3.000\times10^{-6}}$***	9.610×10^{-1}	5.945×10^{-1}	7.579×10^{-1}	7.238×10^{-1}	3.940×10^{-1}	6.845×10^{-1}	9.986×10^{-1}	9.404×10^{-1}	6.234×10^{-1}
NL-SL	$\mathbf{6.490\times10^{-13}}$***	$\mathbf{6.294\times10^{-13}}$***	$\mathbf{6.718\times10^{-13}}$***	9.558×10^{-1}	4.339×10^{-1}	8.659×10^{-1}	8.742×10^{-1}	3.956×10^{-1}	8.159×10^{-1}	9.566×10^{-1}	5.423×10^{-1}	9.082×10^{-1}
LL-ML	1.316×10^{-1}	2.460×10^{-1}	3.116×10^{-1}	9.280×10^{-2}	7.107×10^{-1}	6.593×10^{-1}	6.866×10^{-1}	5.229×10^{-1}	7.948×10^{-1}	9.994×10^{-1}	9.556×10^{-1}	9.600×10^{-1}
LL-SL	$\mathbf{4.24\times10^{-2}}$*	$\mathbf{3.240\times10^{-2}}$*	$\mathbf{2.61\times10^{-2}}$*	9.801×10^{-1}	7.319×10^{-1}	7.153×10^{-1}	8.119×10^{-1}	5.253×10^{-1}	9.049×10^{-1}	9.962×10^{-1}	9.955×10^{-1}	4.424×10^{-1}
ML-SL	1.913×10^{-1}	6.540×10^{-2}	$\mathbf{4.190\times10^{-2}}$*	4.249×10^{-1}	9.809×10^{-1}	9.612×10^{-1}	8.917×10^{-1}	9.998×10^{-1}	9.493×10^{-1}	9.883×10^{-1}	9.950×10^{-1}	4.784×10^{-1}

ΔB_CON	ΔG_CON	ΔR_CON	ΔNIR_CON	ΔB_ENT	ΔG_ENT	ΔR_ENT	ΔNIR_ENT	ΔB_SEM	ΔG_SEM	ΔR_SEM	ΔNIR_SEM	ΔB_COR	ΔG_COR	ΔR_COR	ΔNIR_COR	ΔB_DIS	ΔG_DIS	R_DIS	NIR_DIS
9.865×10^{-1}	8.942×10^{-1}	7.828×10^{-1}	6.319×10^{-1}	9.865×10^{-1}	9.871×10^{-1}	8.970×10^{-1}	4.492×10^{-1}	9.876×10^{-1}	9.941×10^{-1}	9.965×10^{-1}	3.611×10^{-1}	9.884×10^{-1}	9.909×10^{-1}	9.997×10^{-1}	2.648×10^{-1}	9.987×10^{-1}	9.827×10^{-1}	9.999×10^{-1}	4.938×10^{-1}
6.636×10^{-1}	7.955×10^{-1}	8.765×10^{-1}	9.928×10^{-1}	6.793×10^{-1}	9.857×10^{-1}	9.998×10^{-1}	7.634×10^{-1}	7.186×10^{-1}	9.989×10^{-1}	8.587×10^{-1}	9.697×10^{-1}	7.271×10^{-1}	8.526×10^{-1}	5.782×10^{-1}	6.918×10^{-1}	9.573×10^{-2}	6.840×10^{-1}	2.430×10^{-1}	1.418×10^{-1}
4.865×10^{-1}	6.289×10^{-1}	7.684×10^{-1}	5.638×10^{-1}	7.119×10^{-1}	9.967×10^{-1}	9.899×10^{-1}	7.344×10^{-1}	9.765×10^{-1}	1.442×10^{-1}	5.019×10^{-1}	6.557×10^{-1}	9.997×10^{-1}	1.761×10^{-1}	5.762×10^{-1}	7.907×10^{-1}	9.981×10^{-1}	5.016×10^{-1}	5.570×10^{-1}	8.970×10^{-2}
7.551×10^{-1}	6.653×10^{-1}	6.606×10^{-1}	7.222×10^{-1}	7.876×10^{-1}	9.628×10^{-1}	9.625×10^{-1}	9.530×10^{-1}	7.900×10^{-1}	9.916×10^{-1}	9.743×10^{-1}	8.592×10^{-1}	8.233×10^{-1}	8.377×10^{-1}	7.636×10^{-1}	9.976×10^{-1}	9.998×10^{-1}	7.435×10^{-1}	7.744×10^{-1}	9.893×10^{-1}
6.456×10^{-1}	5.039×10^{-1}	5.400×10^{-1}	2.955×10^{-1}	8.612×10^{-1}	9.792×10^{-1}	9.769×10^{-1}	2.571×10^{-1}	9.619×10^{-1}	3.783×10^{-1}	3.880×10^{-1}	1.317×10^{-1}	9.844×10^{-1}	4.640×10^{-1}	2.802×10^{-1}	1.035×10^{-1}	9.997×10^{-1}	9.964×10^{-1}	7.750×10^{-1}	9.951×10^{-1}
9.943×10^{-1}	9.983×10^{-1}	9.998×10^{-1}	5.435×10^{-1}	9.838×10^{-1}	9.987×10^{-1}	9.983×10^{-1}	4.564×10^{-1}	8.418×10^{-1}	7.041×10^{-1}	6.141×10^{-1}	6.889×10^{-1}	7.712×10^{-1}	9.494×10^{-1}	7.884×10^{-1}	4.183×10^{-1}	9.815×10^{-1}	4.061×10^{-1}	9.994×10^{-1}	9.994×10^{-1}

*, **, and *** indicate 0.05, 0.01, and 0.001 levels of significance.

TABLE XI
CONFUSION MATRIX OF LODGING EXTENTS CLASSIFICATION

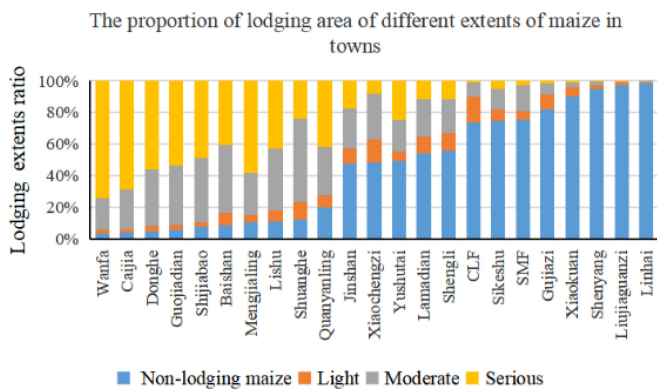|	Training samples					Testing samples				
Class	NL	LL	ML	SL	Total	NL	LL	ML	SL	Total
NL	28	0	0	0	28	17	0	0	0	17
LL	2	3	0	0	5	3	2	0	0	5
ML	0	0	5	0	5	0	0	3	1	4
SL	0	0	1	21	22	0	0	1	13	14
Total	30	3	6	21	60	20	2	4	14	40
	TA: 95.00%, K: 0.93					TA: 87.50%, K: 0.83				

Total accuracy: TA, Kappa Coefficient: K.

Fig. 11.   Proportion of the lodging extents of maize in various towns.

rain was heavy and continuous. Maysak strongly affected maize crop in the central and southern parts of Lishu. The lodging of maize crop was more severe in the southeast and middle of Lishu than in the north and northwest. This is consistent with the result of lodging classification.

V. DISCUSSION

Lodging is one of the common phenomena in maize production, which is mainly caused by strong wind and rainstorms. Remote sensing technology has been widely used in maize lodging monitoring, including optical remote sensing [36], [44], radar remote sensing [29], [35], and UAV remote sensing [6], [15]. Previous researches mainly focused on monitoring the range of maize lodging [36], [37]. How to monitor the lodging extents is of great significance for accurate settlement of insurance claims. In the article, a method for monitoring the lodging extents using remote sensing images before and after lodging was developed. Through the method of RFE, nine sensitive features of lodging extents were screened from the differences of spectrum, texture, and vegetation indices before and after lodging were developed. Through the method of RFE, nine sensitive features of lodging extents were screened from the differences of spectrum, texture and vegetation indices before and after lodging. The results indicated that the method of screening sensitive feature combinations for classification can effectively monitor the lodging extents of maize crop at a large scale. Our accuracy was improved compared with other studies [44], [69].

County-scale lodging monitoring is difficult because of wide range and complex lodging situations. It will take a lot of time and resources to monitor lodging at county scale, either manually or by UAV [11]. The GF-1 image with medium resolution combines the advantages of temporal and spatial resolution. The article proved the feasibility of multitemporal image with medium resolution for monitoring maize lodging at the country scale. The method of monitoring maize lodging proposed in the study is suitable for other satellite images with similar parameters to GF-1 images. After lodging, the weather was many cloudy and rainy. The SAR images are not affected by clouds and fog and are suitable for monitoring crop lodging in extreme weather. In the next step, we will try to combine multispectral images with SAR images to monitor maize lodging.

We used RFECV and MI to select the most sensitive feature combination for monitoring maize crop lodging. RFECV selected 9 features, MI selected 33 features, and the accuracy of CV was less than RFECV. The reason for this phenomenon may be that the correlation between features is high and the selected features are redundant. And RFECV is a kind of embedded method, which associates feature selection with classifier to select the feature combination that is more suitable for the RF classifier [61].

In this article, the resolution of the remote sensing images was 16 m with many mixed pixels between lodging and NL maize, maize crop, and other ground features. One pixel was the combined reflectance of all features within 256 m^2. The higher the resolution of remote sensing image is, the better the classification effect is. The more complex the ground object, the worse the classification result. There were many mixed pixels at the junction of maize crop and other ground objects, which led to low classification accuracy. We will decompose the mixed pixels using adaptive coherence estimator and orthogonal subspace projection to achieve more accurate monitoring of maize lodging extents in the future.

In the testing samples, only two samples were LL. According to the guidance of local agronomic experts, we have conducted full research on the whole study area. The collected samples including maize crop samples and nonmaize samples were distributed throughout the study area, as shown in Fig. 1. In the actual sampling, we found that ML and SL accounted for a larger proportion. LL is too rare to obtain enough samples. We will pay attention to the reasonable sample size in the future lodging monitoring by remote sensing.

VI. CONCLUSION

In this article, the changes of spectrum, vegetation index, and texture features of maize crop were analyzed before and after lodging. The optimal feature combination sensitive to lodging extents was obtained, and the monitoring of maize crop lodging at county scale was realized. The results are as follows:

1) After feature analysis, the sensitive features with lodging extents on maize crop were ΔR_{blue}, ΔR_{green}, ΔR_{red}, ΔNDVI, ΔRVI, ΔEVI, ΔB_MEA, ΔG_MEA, and ΔR_MEA.
2) RFECV selected nine features and achieved higher accuracy than MI. And the results were consistent with feature analysis. The optimal feature combination included ΔR_{blue}, ΔR_{green}, ΔR_{red}, ΔNDVI, ΔRVI, ΔEVI, ΔB_MEA, ΔG_MEA, and ΔR_MEA.
3) The RF classifier was used to classify the optimal feature combination. The classification accuracy was 87.50%, and the kappa coefficient was 0.83 for testing samples.

REFERENCES

[1] L. Chen *et al.*, "Disclosing the future food security risk of China based on crop production and water scarcity under diverse socioeconomic and climate scenarios," *Sci. Total Environ.*, vol. 790, Oct. 2021, Art. no. 148110, doi: 10.1016/j.scitotenv.2021.148110.

[2] P. M. Berry and J. Spink, "Predicting yield losses caused by lodging in wheat," *Field Crops Res.*, vol. 137, pp. 19–26, Oct. 2012, doi: 10.1016/j.fcr.2012.07.019.

[3] P. M. Berry *et al.*, "Understanding and reducing lodging in cereals," in *Advances in Agronomy*, vol. 84, D. L. Sparks, Ed. San Diego, CA, USA: Elsevier, 2004, pp. 217–271, doi: 10.1016/S0065-2113(04)84005-7.

[4] M. S. Islam, S. Peng, R. M. Visperas, N. Ereful, M. S. U. Bhuiya, and A. W. Julfiquar, "Lodging-related morphological traits of hybrid rice in a tropical irrigated ecosystem," *Field Crops Res.*, vol. 101, no. 2, pp. 240–248, Mar. 2007, doi: 10.1016/j.fcr.2006.12.002.

[5] J. Xue *et al.*, "Effects of light intensity within the canopy on maize lodging," *Field Crops Res.*, vol. 188, pp. 133–141, Mar. 2016, doi: 10.1016/j.fcr.2016.01.003.

[6] M.-D. Yang, K.-S. Huang, Y.-H. Kuo, H. P. Tsai, and L.-M. Lin, "Spatial and spectral hybrid image classification for rice lodging assessment through UAV imagery," *Remote Sens.*, vol. 9, no. 6, Jun. 2017, Art. no. 583, doi: 10.3390/rs9060583.

[7] S. Chauhan, R. Darvishzadeh, M. Boschetti, M. Pepe, and A. Nelson, "Remote sensing-based crop lodging assessment: Current status and perspectives," *ISPRS-J. Photogramm. Remote Sens.*, vol. 151, pp. 124–140, May 2019, doi: 10.1016/j.isprsjprs.2019.03.005.

[8] R. T. Ogden, C. E. Miller, K. Takezawa, and S. Ninomiya, "Functional regression in crop lodging assessment with digital images," *J. Agricultural Biol. Environ. Statist.*, vol. 7, no. 3, pp. 389–402, Sep. 2002, doi: 10.1198/108571102339.

[9] L. Zhao, J. Yang, P. Li, L. Shi, and L. Zhang, "Characterizing lodging damage in wheat and canola using radarsat-2 polarimetric SAR data," *Remote Sens. Lett.*, vol. 8, no. 7, pp. 667–675, 2017, doi: 10.1080/2150704X.2017.1312028.

[10] F. Wu, C. Wang, H. Zhang, B. Zhang, and Y. Tang, "Rice crop monitoring in south China with RADARSAT-2 quad-polarization SAR data," *IEEE Geosci. Remote Sens. Lett.*, vol. 8, no. 2, pp. 196–200, Mar. 2011, doi: 10.1109/LGRS.2010.2055830.

[11] X. Zhao *et al.*, "Use of unmanned aerial vehicle imagery and deep learning UNet to extract rice lodging," *Sensors*, vol. 19, no. 18, Sep. 2019, Art. no. 3859, doi: 10.3390/s19183859.

[12] R. M. Haralick, "Statistical and structural approaches to texture," *Proc. IEEE*, vol. 67, no. 5, pp. 786–804, May 1979, doi: 10.1109/PROC.1979.11328.

[13] Q. Sun, L. Sun, M. Shu, X. Gu, G. Yang, and L. Zhou, "Monitoring maize lodging grades via unmanned aerial vehicle multispectral image," *Plant Phenomics*, vol. 2019, 2019, Art. no. 5704154, doi: 10.34133/2019/5704154.

[14] T. Murakami, M. Yui, and K. Amaha, "Canopy height measurement by photogrammetric analysis of aerial images: Application to buckwheat (Fagopyrum esculentum moench) lodging evaluation," *Comput. Electron. Agricultural*, vol. 89, pp. 70–75, Nov. 2012, doi: 10.1016/j.compag.2012.08.003.

[15] W. Su *et al.*, "Phenotyping of corn plants using unmanned aerial vehicle (UAV) images," *Remote Sens.*, vol. 11, no. 17, Sep. 2019, Art. no. 2021, doi: 10.3390/rs11172021.

[16] N. Wilke *et al.*, "Quantifying lodging percentage and lodging severity using a UAV-based canopy height model combined with an objective threshold approach," *Remote Sens.*, vol. 11, no. 5, Mar. 2019, Art. no. 515, doi: 10.3390/rs11050515.

[17] T. Sakamoto *et al.*, "Detecting seasonal changes in crop community structure using day and night digital images," *Photogramm. Eng. Remote Sens.*, vol. 76, no. 6, pp. 713–726, Jun. 2010, doi: 10.14358/PERS.76.6.713.

[18] Z. Liu *et al.*, "Comparison of spectral indices and principal component analysis for differentiating lodged rice crop from normal ones," in *Computer and Computing Technologies in Agriculture V*, vol. 369, D. Li and Y. Chen, Eds. Berlin, Germany: Springer, 2012, pp. 84–92, doi: 10.1007/978-3-642-27278-3_10.

[19] S. Nebikera, A. Annena, M. Scherrerb, and D. Oeschc, "A lightweight multispectral sensor for micro UAV—Opportunities for very high resolution airborne remote sensing," *Int. Arch. Photogramm., Remote Sens. Spatial Inf. Sci.*, vol. 37, no. Part B1, pp. 1193–1200, 2008.

[20] C. A. F. Ezequiel *et al.*, "UAV aerial imaging applications for post-disaster assessment, environmental management and infrastructure development," in *Proc. Int. Conf. Unmanned Aircr. Syst.*, 2014, pp. 274–283, doi: 10.1109/ICUAS.2014.6842266.

[21] C. Zhang, D. Walters, and J. M. Kovacs, "Applications of low altitude remote sensing in agriculture upon farmers' requests—A case study in Northeastern Ontario, Canada," *PLoS One*, vol. 9, no. 11, Art. no. e112894, Nov. 2014, doi: 10.1371/journal.pone.0112894.

[22] H. Y. Liu, G. J. Yang, and H. C. Zhu, "The extraction of wheat lodging area in UAV's image used spectral and texture features," *Appl. Mech. Mater.*, vol. 651–653, pp. 2390–2393, 2014, doi: 10.4028/www.scientific.net/AMM.651-653.2390.

[23] S. C. Chapman *et al.*, "Pheno-Copter: A low-altitude, autonomous remote-sensing robotic helicopter for high-throughput field-based phenotyping," *Agronomy*, vol. 4, no. 2, Jun. 2014, Art. no. 2, doi: 10.3390/agronomy4020279.

[24] T. Chu, M. J. Starek, M. J. Brewer, S. C. Murray, and L. S. Pruter, "Assessing lodging severity over an experimental maize (Zea mays L.) Field using UAS images," *Remote Sens.*, vol. 9, no. 9, Sep. 2017, Art. no. 9, doi: 10.3390/rs9090923.

[25] T. Liu *et al.*, "Estimates of rice lodging using indices derived from UAV visible and thermal infrared images," *Agricultural Forest Meteorol.*, vol. 252, pp. 144–154, Apr. 2018, doi: 10.1016/j.agrformet.2018.01.021.

[26] B. A. M. Bouman, "Crop parameter estimation from ground-based x-band (3-cm wave) radar backscattering data," *Remote Sens. Environ.*, vol. 37, no. 3, pp. 193–205, Sep. 1991, doi: 10.1016/0034-4257(91)90081-G.

[27] B. A. M. Bouman and H. W. J. van Kasteren, "Ground-based X-band (3-cm wave) radar backscattering of agricultural crops Part - II. Wheat, barley, and oats; the impact of canopy structure," *Remote Sens. Environ.*, vol. 34, no. 2, pp. 107–119, Nov. 1990, doi: 10.1016/0034-4257(90)90102-R.

[28] B. A. M. Bouman and H. W. J. van Kasteren, "Ground-based X-band (3-cm wave) radar backscattering of agricultural crops Part - I. Sugar beet and potato; backscattering and crop growth," *Remote Sens. Environ.*, vol. 34, no. 2, pp. 93–105, Nov. 1990, doi: 10.1016/0034-4257(90)90101-Q.

[29] J. Chen, H. Li, and Y. Han, "Potential of RADARSAT-2 data on identifying sugarcane lodging caused by Typhoon," in *Proc. 5th Int. Conf. Agro-Geoinf.*, 2016, pp. 1–6, doi: 10.1109/Agro-Geoinformatics.7577665.

[30] W. Wu, W. Wang, M. E. Meadows, X. Yao, and W. Peng, "Cloud-based typhoon-derived paddy rice flooding and lodging detection using multi-temporal Sentinel-1&2," front," *Earth Sci.*, vol. 13, no. 4, Dec. 2019, Art. no. 4, doi: 10.1007/s11707-019-0803-7.

[31] L. Zhao, J. Yang, P. Li, L. Shi, and L. Zhang, "Characterizing lodging damage in wheat and canola using radarsat-2 polarimetric SAR data," *Remote Sens. Lett.*, vol. 8, no. 7, pp. 667–675, 2017, doi: 10.1080/2150704X.2017.1312028.

[32] H. Yang *et al.*, "Wheat lodging monitoring using polarimetric index from RADARSAT-2 data," *Int. J. Appl. Earth Observ. Geoinf.*, vol. 34, pp. 157–166, Feb. 2015, doi: 10.1016/j.jag.2014.08.010.

[33] D. Han, H. Yang, G. Yang, and C. Qiu, "Monitoring model of corn lodging based on sentinel-1 radar image," in *Proc. SAR Big Data Era: Models, Methods Appl.*, 2017, pp. 1–5, doi: 10.1109/BIGSARDATA.2017.8124928.

[34] M. Shu *et al.*, "Monitoring of maize lodging using multi-temporal sentinel-1 SAR data," *Adv. Space Res.*, vol. 65, no. 1, pp. 470–480, Jan. 2020, doi: 10.1016/j.asr.2019.09.034.

[35] S. Chauhan, R. Darvishzadeh, M. Boschetti, and A. Nelson, "Estimation of crop angle of inclination for lodged wheat using multi-sensor SAR data," *Remote Sens. Environ.*, vol. 236, Jan. 2020, Art. no. 111488, doi: 10.1016/j.rse.2019.111488.

[36] Y. Chen *et al.*, "A simple and robust spectral index for identifying lodged maize using Gaofen-1 satellite data," *Sensors*, vol. 22, no. 3, Feb. 2022, Art. no. 989, doi: 10.3390/s22030989.

[37] J. Wang *et al.*, "Analysis of combining SAR and optical optimal parameters to classify typhoon-invasion lodged rice: A case study using the random forest method," *Sensors*, vol. 20, no. 24, Dec. 2020, Art. no. 7346, doi: 10.3390/s20247346.

[38] Z. Wang *et al.*, "Detection and analysis of degree of maize lodging using UAV-RGB image multi-feature factors and various classification methods," *ISPRS Int. J. Geo-Inf.*, vol. 10, no. 5, May 2021, Art. no. 309, doi: 10.3390/ijgi10050309.

[39] M. Brunato and R. Battiti, "X-MIFS: Exact mutual information for feature selection," in *Proc. Int. Joint Conf. Neural Netw.*, 2016, pp. 3469–3476, doi: 10.1109/IJCNN.2016.7727644.

[40] C. T. Tran, M. Zhang, P. Andreae, and B. Xue, "A wrapper feature selection approach to classification with missing data," in *Proc. Eur. Conf. Appl. Evol. Comput.*, 2016, pp. 685–700, doi: 10.1007/978-3-319-31204-0_44.

[41] R. Setiono and H. Liu, "Neural-network feature selector," *IEEE Trans. Neural Netw.*, vol. 8, no. 3, pp. 654–662, May 1997, doi: 10.1109/72.572104.

[42] S.-Y. Shao, K.-Q. Shen, C.-J. Ong, X.-P. Li, and E. P. V. Wilder-Smith, "Automatic identification and removal of artifacts in EEG using a probabilistic multi-class SVM approach with error correction," in *Proc. IEEE Int. Conf. Syst., Man Cybern.*, 2008, pp. 1134–1139, doi: 10.1109/IC-SMC.2008.4811434.

[43] C. Royo, N. Aparicio, D. Villegas, J. Casadesus, P. Monneveux, and J. L. Araus, "Usefulness of spectral reflectance indices as durum wheat yield predictors under contrasting Mediterranean conditions," *Int. J. Remote Sens.*, vol. 24, no. 22, pp. 4403–4419, Nov. 2003, doi: 10.1080/0143116031000150059.

[44] L. Zhou et al., "Remote sensing of regional-scale maize lodging using multitemporal GF-1 images," *J. Appl. Remote Sens.*, vol. 14, no. 1, Feb. 2020, Art. no. 014514, doi: 10.1117/1.JRS.14.014514.

[45] P. Hao, "Early-season crop type mapping using 30-m reference time series (vol 19, pg 1897, 2020)," *J. Integrative Agriculture*, vol. 20, no. 10, pp. 1897–1911, Oct. 2021.

[46] A. Chen, T. C. Lantz, T. Hermosilla, and M. A. Wulder, "Biophysical controls of increased tundra productivity in the Western Canadian arctic," *Remote Sens. Environ.*, vol. 258, Jun. 2021, Art. no. 112358, doi: 10.1016/j.rse.2021.112358.

[47] H. Peng-yu, T. Hua-jun, C. Zhong-xin, Y. Le, and W. Ming-quan, "High resolution crop intensity mapping using harmonized landsat-8 and sentinel-2 data," *J. Integrative Agriculture*, vol. 18, no. 12, pp. 2883–2897, Dec. 2019, doi: 10.1016/S2095-3119(19)62599-2.

[48] L. Zhang et al., "Identification of seed maize fields with high spatial resolution and multiple spectral remote sensing using random forest classifier," *Remote Sens.*, vol. 12, no. 3, Feb. 2020, Art. no. 362, doi: 10.3390/rs12030362.

[49] E. Romano, S. Bergonzoli, I. Pecorella, C. Bisaglia, and P. De Vita, "Methodology for the definition of durum wheat yield homogeneous zones by using satellite spectral indices," *Remote Sens.*, vol. 13, no. 11, Jun. 2021, Art. no. 2036, doi: 10.3390/rs13112036.

[50] C. F. Jordan, "Derivation of leaf-area index from quality of light on the forest floor," *Ecology*, vol. 50, no. 4, pp. 663–666, Jul. 1969, doi: 10.2307/1936256.

[51] J. W. Rouse et al., "Monitoring the vernal advancement and retrogradation (green wave effect) of natural vegetation," Jan. 1973, Art. no. RSC-1978-2. Accessed: Mar. 8, 2022. [Online]. Available: https://ntrs.nasa.gov/citations/1974000492

[52] Y. J. Kaufman and D. Tanre, "Atmospherically resistant vegetation index (ARVI) for EOS-MODIS," *IEEE Trans. Geosci. Remote Sens.*, vol. 30, no. 2, pp. 261–270, Mar. 1992, doi: 10.1109/36.134076.

[53] R. H. Waring, N. C. Coops, W. Fan, and J. M. Nightingale, "MODIS enhanced vegetation index predicts tree species richness across forested ecoregions in the contiguous USA," *Remote Sens. Environ.*, vol. 103, no. 2, pp. 218–226, Jul. 2006, doi: 10.1016/j.rse.2006.05.007.

[54] J. Penuelas, B. Frederic, and I. Filella, "Semi-empirical indices to assess Carotenoids/Chlorophyll-a ratio from leaf spectral reflectance," *Photosynthetica*, vol. 31, pp. 221–230, Jan. 1995.

[55] W.-Y. Chang, J.-C. Ma, H.-T. Chiu, K.-C. Lin, and P.-H. Lee, "Job satisfaction and perceptions of quality of patient care, collaboration and teamwork in acute care hospitals," *J. Adv. Nurs.*, vol. 65, no. 9, pp. 1946–1955, Sep. 2009, doi: 10.1111/j.1365-2648.2009.05085.x.

[56] C. Wang, Z. Xiao, and J. Wu, "Functional connectivity-based classification of autism and control using SVM-RFECV on RS-fMRI data," *Phys. Med.*, vol. 65, pp. 99–105, Sep. 2019, doi: 10.1016/j.ejmp.2019.08.010.

[57] G. Louppe, "Understanding random forests: From theory to practice," Jul. 2014. Accessed: Mar. 08, 2022. [Online]. Available: https://ui.adsabs.harvard.edu/abs/2014arXiv1407.7502L

[58] Q. Zhang, P. Liu, X. Wang, Y. Zhang, Y. Han, and B. Yu, "StackPDB: Predicting DNA-binding proteins based on XGB-RFE feature optimization and stacked ensemble classifier," *Appl. Soft Comput.*, vol. 99, Feb. 2021, Art. no. 106921, doi: 10.1016/j.asoc.2020.106921.

[59] A. Soltani et al., "Algorithms for walking speed estimation using a lower-back-worn inertial sensor: A cross-validation on speed ranges," *IEEE Trans. Neural Syst. Rehabil. Eng.*, vol. 29, pp. 1955–1964, 2021, doi: 10.1109/TNSRE.2021.3111681.

[60] S. Raschka, "Model evaluation, model selection, and algorithm selection in machine learning," Nov. 2018, doi: 10.48550/arXiv.1811.12808.

[61] H. Peng, F. Long, and C. Ding, "Feature selection based on mutual information criteria of max-dependency, max-relevance, and min-redundancy," *IEEE Trans. Pattern Anal. Mach. Intell.*, vol. 27, no. 8, pp. 1226–1238, Aug. 2005, doi: 10.1109/TPAMI.2005.159.

[62] L. Breiman, "Random forests," *Mach. Learn.*, vol. 45, no. 1, pp. 5–32, Oct. 2001, doi: 10.1023/A:1010933404324.

[63] F. Jiang, M. Kutia, K. Ma, S. Chen, J. Long, and H. Sun, "Estimating the aboveground biomass of coniferous forest in Northeast China using spectral variables, land surface temperature and soil moisture," *Sci. Total Environ.*, vol. 785, Sep. 2021, Art. no. 147335, doi: 10.1016/j.scitotenv.2021.147335.

[64] B. R. de Oliveira et al., "Eucalyptus growth recognition using machine learning methods and spectral variables," *Forest Ecol. Manage.*, vol. 497, Oct. 2021, Art. no. 119496, doi: 10.1016/j.foreco.2021.119496.

[65] X. Chen and H. Ishwaran, "Random forests for genomic data analysis," *Genomics*, vol. 99, no. 6, pp. 323–329, Jun. 2012, doi: 10.1016/j.ygeno.2012.04.003.

[66] S. Van der Linden et al., "The EnMAP-Box—A toolbox and application programming interface for EnMAP data processing," *Remote Sens.*, vol. 7, no. 9, Sep. 2015, Art. no. 9, doi: 10.3390/rs70911249.

[67] Q. Sun et al., "Monitoring maize canopy chlorophyll density under lodging stress based on UAV hyperspectral imagery," *Comput. Electron. Agriculture*, vol. 193, Feb. 2022, Art. no. 106671, doi: 10.1016/j.compag.2021.106671.

[68] L. J. Li et al., "Dual application of ethephon and DCPTA increases maize yield and stalk strength," *Agronomy J.*, vol. 111, no. 2, pp. 612–627, Apr. 2019, doi: 10.2134/agronj2018.06.0363.

[69] A. Chakraborty, P. Srikanth, C. S. Murthy, P. V. N. Rao, and S. Chowdhury, "Assessing lodging damage of jute crop due to super cyclone amphan using multi-temporal sentinel-1 and sentinel-2 data over parts of West Bengal, India," *Environ. Monit. Assessment*, vol. 193, no. 8, Jul. 2021, Art. no. 464, doi: 10.1007/s10661-021-09220-w.

Xuzhou Qu received the B.S. degree in spatial information and digital technology from the School of Remote Sensing and Information Engineering, North China Institute of Aerospace Engineering, Langfang, China, in 2020. He is currently working toward the post graduate's degree in cartography and geography information system with the School of Geoscience, Yangtze University, Jingzhou, China.

His research interest includes agricultural disaster remote sensing.

Dong Shi received the Ph.D. degree in photogrammetry and remote sensing from the State Key Laboratory of Photogrammetry and Remote Sensing, Wuhan University, Wuhan, China, in 2006.

Her research interests include GIS application, digital earth, logging geology, and reservoir description.

Xiaohe Gu received the Ph.D. degree in cartography and geographic information system from the School of Resources, Beijing Normal University, Beijing, China, in 2006.

He is currently a Researcher with the Research Center of Information Technology, Beijing Academy of Agriculture and Forestry Sciences, Beijing, China. His research interests include remote sensing in agriculture and ecology, including remote sensing assessment of rice flood disaster, crop growth monitoring and yield estimation, and remote sensing monitoring of cultivated land quality.

Qian Sun received the master's degree from the College of Geomatics, Shandong University of Science and Technology, Qingdao, China, in 2020. She is currently working toward the Doctoral degree with the College of Information and Electrical Engineering, China Agricultural University, Beijing, China.

She is currently studying at the Research Center of Information Technology, Beijing Academy of Agriculture and Forestry Sciences, Beijing, China. Her research interest is agricultural remote sensing application research, with focus on crop lodging monitoring and crop stress.

Xueqian Hu was received the B.S. degree in remote sensing science and technology from the School of Surveying and Mapping and Spatial Information, Shandong University of Science and Technology, Qingdao, China, in 2019. He is currently working toward the post graduate's degree in photography and remote sensing with the School of Surveying and Mapping and Spatial Information, Shandong University of Science and Technology.

His research interests include crop lodging monitoring based on remote sensing.

Xin Yang received the B.S. degree in mathematics and applied mathematics from the School of Science, Hebei University of Science and Technology, Shijiazhuang, China, in 2020. He is currently working toward the postgraduate degree in mathematics from the School of Science, China University of Geosciences, Beijing, China.

His research interests include deep learning and intelligent algorithms.

Yuchun Pan received the master's degree in cartography and remote sensing from the Northeast Institute of Geography and Agroecology, Chinese Academy of Sciences, Beijing, China, in 1999.

In 2002, he graduated from the Institute of Geographical Sciences and Resources, Chinese Academy of Sciences, and obtained a doctorate in cartography and geographic information system. After graduating in 2002, he worked with the Beijing Agricultural Information Technology Research Center. In the same year, he was included in the Beijing Excellent Talents Training Plan, and in 2006, he was selected into Beijing Science and Technology Nova Training Plan. He was the Director of the Beijing Agricultural Products Quality and Safety Society and the Director of Beijing Geographical Society. He is mainly engaged in spatial information technology and its application research. His research interests include the theoretical and technical methods of agricultural resources and environmental information acquisition, sampling layout optimization, spatiotemporal data mining analysis, agricultural and land resource quality evaluation and planning, agricultural disaster and emergency risk assessment, and resource optimal allocation.